Supporting Material

Cell Volume Fluctuations in MDCK Monolayers

Steven M. Zehnder,[*] Melanie Suaris,[†] Madisonclaire M. Bellaire,[‡] and Thomas E. Angelini,[*†¶]

[*]Department of Mechanical and Aerospace Engineering, University of Florida, Gainesville, USA; [†]J. Crayton Pruitt Family Department of Biomedical Engineering, University of Florida, Gainesville, USA; [‡]Department of Physics, University of Florida, Gainesville, USA; [¶]Institute for Cell Engineering and Regenerative Medicine, University of Florida, Gainesville, USA

Movie S1

Fluctuations in the projected areas of cells can be seen in time-lapse. At any instant, regions of low number density composed of large cells coexist near regions of high number density composed of small cells. Over time, single cells fluctuate in projected area, sometimes doubling or tripling in size. Cell divisions appear as extremely rapid reductions in cell area compared to area fluctuations between divisions. The fast decrease in area of dividing cells facilitates their identification and rejection from analysis. Scalebar 150 μm.

Cell Culture Protocols and Experimental Details

MDCK epithelial cell layers are plated on glass-bottomed culture dishes coated with collagen I. Cells are cultured in Dulbecco's Modified Eagle Medium (DMEM), 5% fetal bovine serum, 1% penicillin-streptomycin, and maintained at 37 °C and 5% CO_2. For experiments in which cells are fluorescently dyed, cells are treated with 15 μM 5-chloromethylfluorescein diacetate (CMFDA) in serum-free DMEM and 0.15% DMSO for 30 minutes, then returned to full serum-containing DMEM and immediately imaged in time-lapse. For Myosin II inhibition experiments, growth media supplemented with 100μM blebbistatin is used. Cells are transferred to an inverted microscope with automated shuttering and full environmental control. Low light levels are maintained by using a 10% neutral density filter in line with the fluorescence lamp and by opening the shutter for less than 100ms every minute for 9 hours. To eliminate z-drift after a focal plane is chosen, we use an interferometric objective positioning system (Nikon Perfect Focus), which does not rely on any image-based auto-focusing algorithms and maintains focus within a few nanometers along the optical axis. Volume fluctuation measurements of cells with and without blebbistatin treatment were repeated three times, producing consistent results.

Cells are plated as circular islands approximately 5mm in diameter. Cells are deposited at the minimum confluent density, which is just dense enough such that no open space is observed within the layer. Imaging is performed away from the immediate edge of the island in a region where island expansion and cell proliferation nearly balance, and consequently the average cell density rises very slowly. We measured the cell division rate in this system, finding a division time of approximately 40 hours, in agreement with our previous studies. Dividing cells are identified by a large, rapid drop in measured area over the course of about 10-20 minutes; dividing cells are not included in the analysis. A relatively small change in cell density over time is observed at the large scale by measuring the average cell area at each time point (Fig. S1). Traces of individual cell area also show no dramatic transient behavior, though each cell fluctuates substantially over time (Fig. S2). These strong fluctuations in cell area are coupled to local fluctuations in multicellular motion, though we observe no significant collective migration over lengthscales exceeding approximately 200 μm (Video S1). The oscillatory nature of single cell area, averaged over hundreds of cell area traces, is captured by the autocorrelation function, described in the manuscript. In Fourier analysis of signals, the lowest measurable frequency has a corresponding period of twice the sample duration. Thus, for each single 9 hour cell measurement, the minimum measurable frequency increment is 1/18 h^{-1}. The frequency of a 4 hour period is 1/4 h^{-1}, 4.5 times the lowest measureable frequency. The frequency of a 6 hour period is 1/6 h^{-1}, 3 times the lowest measurable frequency. Thus, the period of oscillation measured from correlation functions or Fourier spectra are not limited by the duration of the experiments.

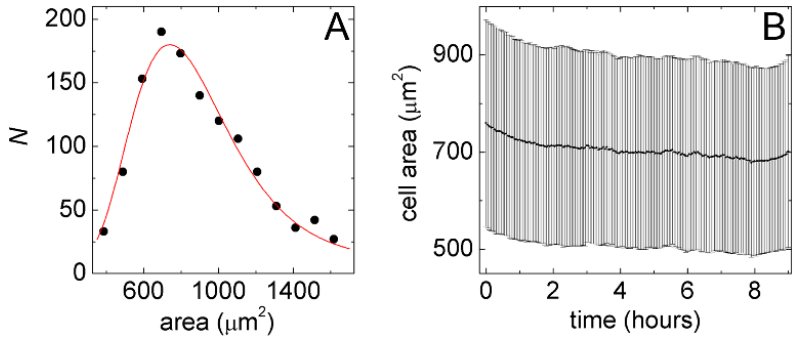

Figure S1. Within each collected frame, the cell area histogram is skewed and is well described by a log-normal distribution (A, dots are data, red line is a log-normal distribution fit). To measure a representative cell area within the monolayer at each time, we estimate the location of the peak in each histogram and a coefficient of variation by using log-normal statistics. The resulting plot of cell area versus time shows a small decrease in average cell area from about 750 μm^2 to just below 700 μm^2, with a very large variation in size at all times (B).

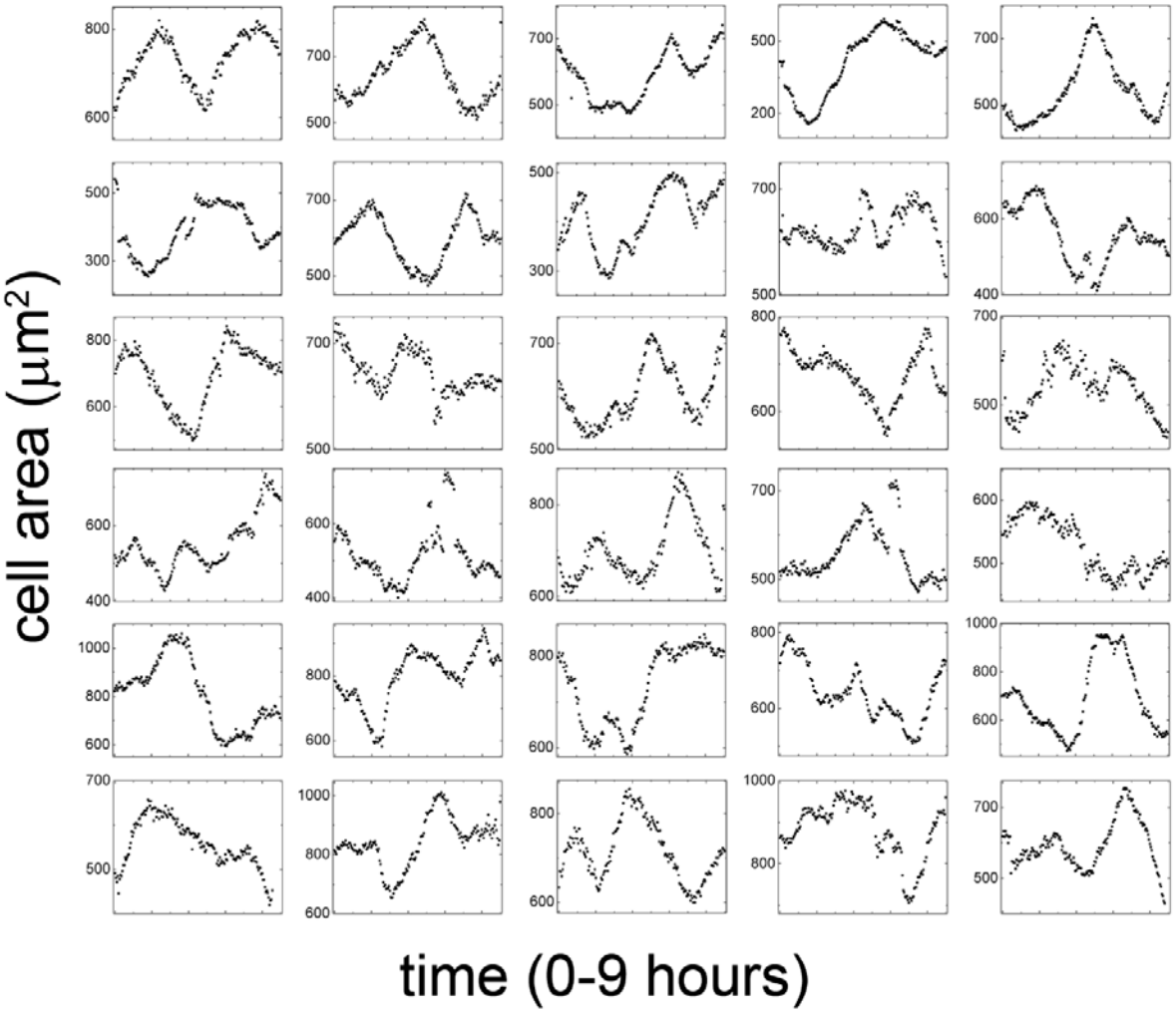

Figure S2. The typical cell fluctuates in area by about ±20% every four hours, performing a full oscillation in about 1/10 of the typical cell division time. Thirty traces of different cell areas versus time show the general oscillatory fluctuating behavior, but individual cells can fluctuate by much more or less than the average, and also oscillate at different rates.

Cell Volume, Area, and Thickness

Measurements of cell thickness variation in time and space, described in the manuscript text, demonstrate that cell thickness fluctuations are small compared to cell area fluctuations. The disparity between cell area fluctuations and cell thickness fluctuations reveals that cell volume fluctuations accompany area fluctuations, though it is unclear whether spreading cells become thinner or thicker, even if the change is small. To test whether spreading cells become thinner and contracting cells become thicker, conserving some fraction of volume, we follow the area, thickness, and volume of several cells in the confocal microscope over time. The cell boundary at each time point is identified by computing an average intensity projection along the z-axis; since a great number of cells possess nearly vertical interfaces, their boundaries are easily identified. The height at every location within the cell boundary is measured in the same way as described in the manuscript, and an average is taken to determine cell thickness at each point in time. The product of the X-Y pixel size and the height at any single location within the cell boundary produces a volume element; the volume of the cell is computed from the sum of all volume elements within the cell boundary.

We find that the instantaneous variation in height across a single cell surface is larger than the change in average height over time. Surprisingly, when tracking changes in a cell with strongly decreasing area, we find that the cell thickness also decreases, exhibiting no sign of volume conservation at all. By contrast, a cell with moderately decreasing area thickens, exhibiting volume conservation. A cell with increasing area was found to exhibit no clear change in thickness. Thus, plots of cell thickness versus volume show no systematic correlation across these different cells. However, plots of area versus volume show strong correlations, suggesting that fluctuations in volume may be approximated by fluctuations in area (Fig. S3).

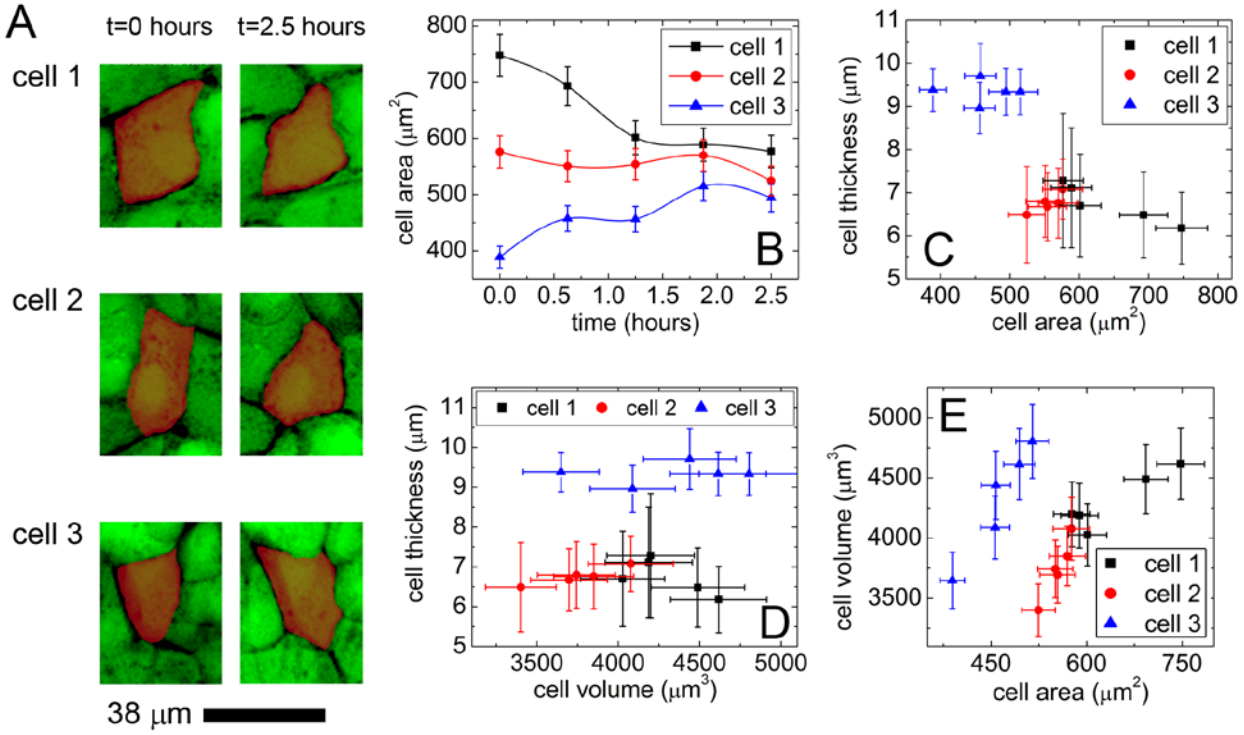

Figure S3. Cell boundaries are identified in z-projections of confocal stacks (A). The cells exhibit different variations in area over time (B, Errorbars: uncertainty estimate of area for precision of 1 pixel). Cell 1 decreases in area and decreases in thickness; cell 2 decreases in area and increases in thickness; cell 3 increases in area and does not change thickness (C, bars are standard deviation of height across the cell surface). There is no systematic change in thickness with volume (D), yet there are strong, systematic correlations between cell area and cell volume (E, volume errorbars: combination of height and area error estimates).

Spatial Correlations in Cell Density and Area

Heterogeneity in cell size appears to occur over a characteristic multi-cellular lengthscale. To quantify these apparent spatial correlations in cell density, we compute a density-density autocorrelation function. With the Voronoi tessellation analysis described in the main text, the area of every cell within the field of view is computed, and a spatial map of area is constructed. The reciprocal of this area map is a map of local number density of cells. We compute the density-density autocorrelation function in 2D, $C_{\sigma\sigma}(\mathbf{R}) = \langle \sigma(\mathbf{r})\sigma(\mathbf{r}+\mathbf{R}) \rangle_{\mathbf{r}}$, where σ is the number density and the angle brackets indicate an average over all locations in space. The 2D correlation function is azimuthally averaged to produce a simple 1D correlation function, $C_{\sigma\sigma}(R) = \langle C_{\sigma\sigma}(\mathbf{R}) \rangle_{\phi}$. We find that $C_{\sigma\sigma}$ decays rapidly out to approximately 75 microns, or 3-4 cell lengths. At larger distances, $C_{\sigma\sigma}$ exhibits a rise and a peak at a lengthscale of about 200 μm, or ten cell lengths. Thus, cell area and number density exhibit a spatial fluctuation on multi-cellular lengthscales. This lengthscale is comparable to spatial correlation lengths observed in migration velocity fields. Thus, a strong coupling between cell density fluctuations and spatial correlation in migration velocity is likely to occur here, and insight may be found in previous work in active particulate systems (2-4).

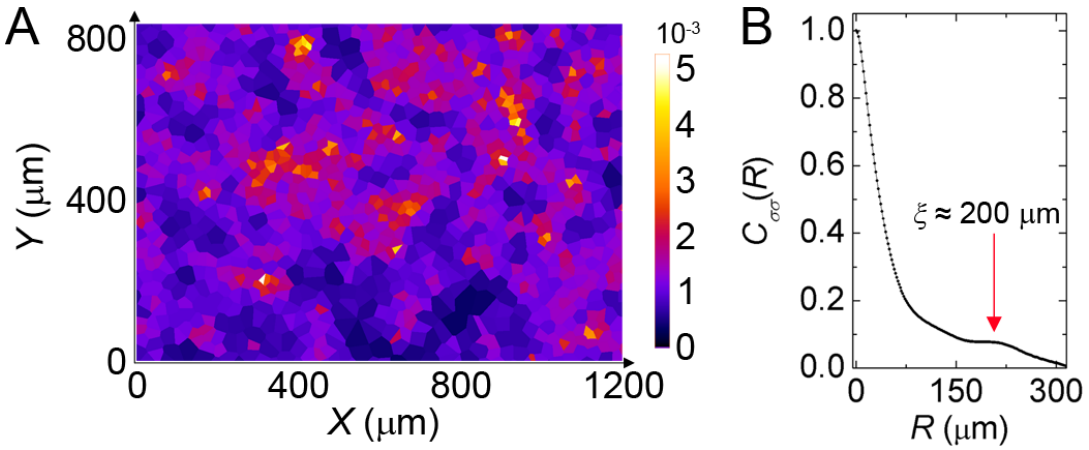

Figure S4. Voronoi tessellations are generated from cell nuclei positions, and individual cell areas are approximated by the corresponding Voronoi cell areas. Cell density, σ, is computed from the reciprocal of cell area (B, intensity bar units are cells per μm^2). The density-density autocorrelation function, $C_{\sigma\sigma}(R)$ exhibits a small peak at R = 200 μm, corresponding to the spacing between regions of similar density.

Gap Junction Permeability

Large assemblies of fluid channels, known as gap junctions, constitute several percent of the cell-cell interface, connecting neighboring cells in tissues and monolayers (5-8). The resistance to pressure-driven flow through gap junctions can be estimated from the dimensions of their channels and the number of open channels that connect cells. From gap junction conductance measurements of MDCK cells and single gap junction channel conductance we estimate that a typical MDCK cell is connected to its neighbors through approximately 2000 open gap junction channels (9,10). Approximating transport through these channels as Poiseuille flow, we predict a permeability, $k = \left(N_c \pi D^4\right) / \left(128 \eta L\right)$, where N_c is the number of channels per cell, D is the diameter of each channel, η is the fluid viscosity, and L is the channel length. For a fluid with the viscosity of water driven through channels of diameter, D = 2 nm, and length, L =16 nm, we find k = 0.06 μm^3 kPa^{-1} s^{-1}. A cell with this permeability could expel 20% of its own volume in two hours by generating only 1.1 kPa of excess pressure, relative to its neighbors. Comparable levels of spatial variability in cell generated normal-stress have been measured in epithelial, endothelial, and cancer cell monolayers. These back-of-the-envelope estimates suggest that the levels of pressure required to drive intercellular fluid flow are modest, and given the ubiquity of gap junctions and contractile force generation in tissue cells, cell volume changes may drive intercellular fluid flow in many systems (5,11,12).

Cytoskeleton Permeability

In order for fluid to flow from cell-to-cell, it must also traverse the cytoskeleton. The permeability of any dense polymer network, including the cytoskeleton, is expected to be excessively low for pressure driven flow, limited by the small mesh-size. To test the cytoskeleton's potential to limit intercellular flow, we estimate the effective permeability of the cytoskeleton to be $k = A\xi^2 / \eta L$, where A is the cell cross sectional area in profile, ξ is the network mesh-size, η is the fluid viscosity, and L is the lateral lengthscale over which the fluid must flow (13). For a cell with an area in profile, $A = hL$, a cell height, h = 7 μm, a mesh size of 100 nm (14-16), and a viscosity, η = 0.89 mPa s, we estimate an effective cytoskeletal permeability of 8×10^4 μm^3 kPa^{-1} s^{-1}, many orders of magnitude larger than the estimated single cell, gap junction permeability. Previous work showed that over short time-scales, less than about a minute, the cytoskeleton permeability limits flow and poroelastic effects dominate (17). However, in our work we observe volume changes over the course of hours and we expect permeability to be further increased over longer time-scales; the cytoskeleton is in constant flux, maintaining cytoskeletal tension while remodeling over times shorter than the volume fluctuations observed here (18).

Membrane and Aquaporin Permeability

Isolated cells under isotonic conditions maintain a constant volume, although applied osmotic pressure can drive fluid across the cell membrane or through aquaporins, generating cell volume change (1). The hydraulic permeability of individual MDCK cells has been measured by monitoring cell volume change under increased osmotic pressure (19). An increase in the osmotic pressure of the growth media by about 200kPa, or 80 mOsm/kg, causes the cells to shrink rapidly over the course of a few minutes, and the MDCK permeability is found to be 2×10^{-8} cm s^{-1} $mOsm^{-1}$ kg. (19). To compare to the permeability estimates above, we multiply this permeability by the measured projected cell area of 700 μm^2 and convert units, finding a permeability of 0.06 μm^3 kPa^{-1} s^{-1}. Interestingly, this permeability is the same as the permeability of cells for flow through gap junctions. When osmotic pressure is applied to cells, they respond by rapidly transferring ions across the membrane with ion pumps, driving water across the cell membrane, recovering most of their equilibrium volume within few minutes (20). This suggests that cells can generate osmotic pressures of at least 100kPa by driving ion transport. Thus, these simple estimates suggest the possibility that cells in monolayers generate the volume fluctuations that we observe here if ion transport oscillates regularly over the course of several hours.

SUPPLEMENTARY REFERENCES

1. Hoffmann, E. K. and L. Simonsen. 1989. Membrane mechanisms in volume and pH regulation in vertebrate cells. Physiol Rev 69:315-382.

2. Henkes, S., Y. Fily, and M. C. Marchetti. 2011. Active jamming: Self-propelled soft particles at high density. Physical Review E 84:040301.

3. Deforet, M., M. C. Parrini, L. Petitjean, M. Biondini, A. Buguin, J. Camonis, and P. Silberzan. 2012. Automated velocity mapping of migrating cell populations (AVeMap). Nature methods 9:1081-1083.

4. Schaller, V. and A. R. Bausch. 2013. Topological defects and density fluctuations in collectively moving systems. Proceedings of the National Academy of Sciences 110:4488-4493.

5. Dermietzel, R. and D. C. Spray. 1993. Gap junctions in the brain: where, what type, how many and why? Trends in Neurosciences 16:186-192.

6. Evans, W. H. and P. E. Martin. 2002. Gap junctions: structure and function (Review). Molecular membrane biology 19:121-136.

7. Meyer, D. J., S. B. Yancey, and J. P. Revel. 1981. Intercellular communication in normal and regenerating rat liver: a quantitative analysis. The Journal of Cell Biology 91:505-523.

8. Caspar, D. L. D., D. A. Goodenough, L. Makowski, and W. C. Phillips. 1977. Gap Junction Structures: I. Correlated Electron Microscopy and X-Ray Diffraction. The Journal of Cell Biology 74:605-628.

9. Bennett, M. and V. Verselis. 1992. Biophysics of gap junctions. Seminars in cell biology 3:29-47.

10. Giaume, C., C. Sahuquillo, D. Louvard, and H. Korn. 1986. Evidence for ionic coupling between MDCK cells at non-confluent and confluent stages of culture. Biology of the Cell 57:33-38.

11. Discher, D. E., P. Janmey, and Y.-l. Wang. 2005. Tissue Cells Feel and Respond to the Stiffness of Their Substrate. Science 310:1139-1143.

12. Larsen, W. J. 1977. Structural diversity of gap junctions. A review. Tissue and Cell 9:373-394.

13. Dullien, F. A. 1991. Porous media: fluid transport and pore structure: Academic press.

14. Howard, J. 2001. Mechanics of motor proteins and the cytoskeleton.

15. Satcher Jr, R. L. and C. F. Dewey Jr. 1996. Theoretical estimates of mechanical properties of the endothelial cell cytoskeleton. Biophysical journal 71:109-118.

16. Medalia, O., I. Weber, A. S. Frangakis, D. Nicastro, G. Gerisch, and W. Baumeister. 2002. Macromolecular architecture in eukaryotic cells visualized by cryoelectron tomography. Science 298:1209-1213.

17. Charras, G. T., J. C. Yarrow, M. A. Horton, L. Mahadevan, and T. Mitchison. 2005. Non-equilibration of hydrostatic pressure in blebbing cells. Nature 435:365-369.

18. Bursac, P., G. Lenormand, B. Fabry, M. Oliver, D. A. Weitz, V. Viasnoff, J. P. Butler, and J. J. Fredberg. 2005. Cytoskeletal remodelling and slow dynamics in the living cell. Nature materials 4:557-561.

19. Timbs, M. and K. Spring. 1996. Hydraulic properties of MDCK cell epithelium. The Journal of membrane biology 153:1-11.

20. Pierce, S. K. and A. D. Politis. 1990. Ca2+-activated cell volume recovery mechanisms. Annual review of physiology 52:27-42.